



Investigating routes performance of flight profile generated based on the off-design point: Elaboration of commercial aircraft-engine pairing

Selcuk Ekici

Department of Aviation, Iğdır University, TR-76000, Iğdır, Turkey

ARTICLE INFO

Article history:

Received 7 November 2019

Received in revised form

13 December 2019

Accepted 17 December 2019

Available online 23 December 2019

Keywords:

Aerospace

Commercial aircraft

Turbofan engine

Gas turbine

Thermodynamic analysis

Exergy analysis

ABSTRACT

In this study, the route performance aspects of B707-JT3D pairing are comprehensively reviewed. A flight route consisting of nine flight operations of the B707-JT3D pairing is defined. The defined flight route was designed to be equivalent to the route a real commercial aircraft is currently exposed to. Parametric cycles were prepared via GasTurb12 software to obtain each flight profile data on the route. The evaluation of the parametric cycle data was carried out by thermodynamic analysis and the performance map of the B707-JT3D pairing is presented. The performance map consists of pressure, temperature, air/fuel mass flow rates, throttle settings, exergy rates, entropy generation rates, exergy efficiency and the exergy destruction function. Ultimately, parameters obtained from the analysis are expected to help understand the linkage between engine selection for commercial aircraft and green flight paths and, therefore, make aircraft-engine pairing more environmentally benign and greener.

© 2019 Elsevier Ltd. All rights reserved.

1. Introduction

1.1. Background information

Aircraft in the transportation sector are a powerful component affecting societies and economies beyond both local and regional political boundaries. Aircraft components and equipment affect communities and economies with regard to environmental effects, sustainability, as well as easy and inexpensive availability in the production/manufacturing/reuse/recycling processes [1].

In the 20th century, customers' expectations from the air transportation sector included travel over a shorter, cheaper and safer time. However, in the 21st century, the fact that humanity has realized serious world climate issues revealed the need to add other factors to the accepted factors prevailing in the aviation sector. One newly-added factor is the greening of the aviation sector. The sector should now be both environmentally sensitive and carry out cheap and safe transportation as soon as possible [2].

In the design of environmentally-conscious aircraft, the analysis of aircraft-engine pairings became a touchstone in the understanding of the impact on the environment as a result of the use of

aircraft. Both the need to select an engine suitable for required operating parameters of aircraft and the need to be appropriate with regard to fuel consumption of the engine in terms of economy and environmental impact have surfaced. The commercial aviation sector wants to increase the efficiency of aircraft-engine pairings within relatively cheap transportation conditions and to reduce fuel consumption in terms of both economy and the environment. Studies aimed at reducing fuel consumption include research on efficient aerodynamic structure, lighter material and more efficient air breathing engines. Thermodynamic analysis has become a useful decision-making tool for the design, the determination of performance parameters and optimization of air breathing engines, which is one of the energy conversion systems [3]. Thermodynamic analysis and optimization have been applied to air vehicle energy conversion systems in order to discover, recognize and produce solutions to combat air vehicle inefficiency. In addition, over the years, thermodynamic analysis has come to be seen as an optimization tool, with thermodynamic optimization having gained a wider place under the title of economic optimization [4].

Aircraft are comprised of various interrelated components consisting of many energy conversion systems. The eventuation of thermodynamic analysis, including energy, exergy, exergo-economy, exergo-environment, and sustainability, at optimization

E-mail address: selcukekici@gmail.com.

and all stages of the aircraft design process, adds an additional perspective to traditional design models. Main engines and APU in aircraft provide the amount of energy the aircraft needs. Briefly, the operating principles of the engines are to obtain high-temperature combustion products by mixing the compressed air in the compressor with the fuel in the combustion chamber. Thus, combustion products obtained at high temperatures expand in the turbine and converted to useful work. Therefore, unlike traditional calculation methods, the use of thermodynamic analysis allows for the calculation and increase of the efficiency of heat engines [5,6]. In addition, thermodynamic analysis is used to understand the theoretical transfer of useful work potential through the components of air breathing engines [7]. The performance evaluation of transferred work potential is also performed through thermodynamic analysis [8].

Energy conversion systems of aircraft are conceptualized with reliance on thermodynamic analysis. In other words, the quality of the energy flow in each component of the aircraft propulsion system has been diagnosable. The combination of the first law of thermodynamics and the second law in the process of diagnosable energy quality provides a map of how much entropy generation can occur in which component of the aircraft engine (*the concept of quality is as important as the quantity of energy*). Entropy generation (*exergy destruction*) in the aircraft-engine relationship occurs due to flow mixing, chemical reaction, rapid compression and expansion processes. Therefore, choosing the appropriate engine for the fuselage (*suitable to maximum takeoff weight, passenger capacity, state of the art technology etc.*) will reduce entropy production and enable more efficient flight operations. Otherwise, unsuitable aircraft-engine interaction, on the basis of the relationship between fuel consumption and thrust, will decrease efficiency, increase any negative environmental impact and will cause economic loss. In order to reduce the negative environmental impact of aircraft and to achieve a sustainable competitive advantage it is necessary to optimize by determining the conditions that will produce minimum entropy generation, or minimum exergy destruction, in the use of aircraft engines, which are energy conversion systems. Conceptualization of exergy destruction, by determining conditions, takes place through 'thermodynamic-based' analysis [9].

Calculating the efficiency of an aircraft-engine pairing through thermodynamic and sustainability analyses has the potential to offer solutions regarding sustainability and environmental effects by determining fuel consumption and engine component performance parameters in all flight phases of the aircraft (LTO^{cycle} 'Landing and Takeoff' and CCD^{stage} 'Climb, Cruise, Descent'). For this reason, thermodynamic analyses of flight phases are investigated by considering aero-engine performance parameters. In this study, a flight route consisting of nine flight operations of a B707-JT3D pairing is defined. Parametric cycles of the JT3D engine at nine flight profiles, depending on altitude and changing ambient conditions, are created via software. The thermodynamic analysis is performed based on data obtained from the cycles and the performance map of the pairing and is presented.

This aircraft-engine pairing study differs from previous studies due to the following features. Furthermore, the differences are discussed comprehensively in the following sections.

- Demonstration of the sensitivity of the thermodynamic analysis to data
- Demonstration that the results can be obtained very far from each other with different thermodynamic analysis methods
- Use of an actual aircraft-engine pairing
- Modeling of nine flight phases

1.2. Previous studies of aircraft-engine pairings at variable altitudes/flight phases/operational modes

There are various studies in the literature in which performance and sustainability parameters of different aircraft engines are determined in a certain condition or under different operating conditions. In the open literature, there are limited articles on thermodynamic analysis of an aircraft-engine pairing at variable conditions. The studies are categorized by year and the necessary explanations are presented below.

Amati et al. [10] designed simulation software to perform thermodynamic analysis in each phase condition depending on different cruise flight phase parameters of the scramjet engine. Designed software is able to analyze the different configurations of the scramjet engine using the exergy approach.

For a turbofan engine, categorized as F100-PW-100 with low bypass ratio developed for the F-15 and F-16 military aircraft, Turgut et al. [11] carried out thermodynamic analysis for atmosphere and engine conditions at sea level and 11 000 m; accepted as cruise altitude. The engine components of the F-15/16-F100-PW-100 pairing were calculated for exergy destruction and improvement potential rates through certain assumptions and theoretically obtained data. Turgut et al. [12] conducted an exergo-economic analysis of an aircraft equipped with a turbofan engine. This introduced a new thermodynamic analysis parameter to the literature that defines the trust cost rate. Turgut et al. [13] performed an exergy analysis of a CF6-80 turbofan engine produced by General Electric. Calculations are based on component data at sea level.

Balli et al. [14] evaluated the thermodynamic analysis of a turbojet engine in accordance with data obtained from a maintenance centre in Turkey. The air breathing engine type discussed in the article is a J69-T 25A and its application on the aircraft is T-37B/C. A thermodynamic analysis of a T-37B/C-J69-T 25A pairing was performed based on the specific environment and conditions of the maintenance center where the particular assumptions and the experimental set-up were installed. Balli and Hepbasli [15] performed both energetic and exergetic analysis of a T56 engine in the turboprop engine category at 75%, 100%, Takeoff and Military operational modes. The thermodynamic analysis method was used in order to determine the performance evaluation parameters of the T56 engine. The study contains both experimental data and theoretical assumptions. The performance parameters were evaluated in terms of fuel exergy depletion, productivity lack, relative exergy consumption at power loads of 75/100/Military/Takeoff which were selected as T56 engine operating modes. Balli [16] determined the sustainability and environmental parameters of a J85 turbojet engine in four different operational modes. In this study, the operational modes that are subject to analysis are defined as Idle, Intermediate, Military and Afterburner. Balli [17] determined the sustainability parameters of a PW4056 turbofan engine used in a commercial aircraft through the thermodynamic model. Analysis of the turbofan engine was performed under different operational modes at sea level. Balli [18] examined the thermodynamic analysis of a turbofan engine in two sections; traditional and advanced. While calculating exergy destruction and entropy generation with a traditional thermodynamic approach, Balli presented a detailed map of exergy destruction with an advanced exergy approach.

Gandolfi et al. [19] conducted thermodynamic analysis of a turbofan engine at six flight phases. The analysis and evaluation parameters were acquired through the GSP (Gas Turbine Simulation Program). The flight phases were defined as takeoff, climb, cruise, descent, holding and landing. The irreversibility was calculated under two different conditions. Struchtrup and Elfring [20] explain the relationship between the bypass ratio and the

components of a turbofan engine through entropy generation/irreversibility. Tona et al. [21] performed thermodynamic analysis of a turbofan engine according to the flight phases. The flight phases were determined as eight stages; takeoff, climb, cruise, descent, holding, and landing. In addition, the study used Matlab and GSP software to determine the performance parameters of the turbofan engine concerning flight phases.

Altuntas et al. [22] conducted a thermodynamic and sustainability analysis of LTO, which is part of the flight operation of an aircraft equipped with a reciprocating engine. Energy, exergy and sustainability analyses were used to determine the performance parameters of the reciprocating engine. In another work, Altuntas et al. [23], conducted a thermodynamic analysis of a reciprocating engine at the cruise stage, which is one of the flight phases. The study presents the results of the analysis at different throttle levels during the cruise flight phase to the literature. Altuntas et al. [24] optimized the performance criteria of a reciprocating engine during the cruise flight phase. This determined air/fuel ratio, power setting and altitudes as the performance criteria.

Aydin et al. [25] carried out an exergo-economic analysis of a turboprop engine used in military transport aircraft CT7-9C by means of the thermodynamic model. The study aimed to reduce operating costs by looking at ways of reducing fuel consumption. Aydin et al. [26] evaluated the sustainability indicators of a PW6000 turbofan engine through the exergetic approach. The indicators were calculated based on the takeoff from the flight phases. Aydin et al. [27] conducted a thermodynamic analysis of a turbofan engine used in commercial aircraft under certain assumptions. Sustainability indicators under the specified environmental conditions for the turbofan engine were revealed.

Turan [28] performed thermodynamic analysis by changing the operating modes of the air breathing engine through certain assumptions and theoretically obtained data. Turan [29] examined the sustainability parameters of a turbofan engine designed as high bypass rate by means of thermodynamic analysis. Analysis based on the data of the engine at the maximum thrust operational mode was carried out. Hassan [30] examined the local entropy generation of a CF6-50 turbofan engine at the intake and fan stations. Therefore, exergy destruction was calculated in certain flow areas through thermal and viscous distributions.

Şöhret et al. [31] conducted a thermodynamic analysis of an UAV equipped with a turbofan engine with a surveillance task requirement. In the study, the component parameters of the turbofan engine were determined according to the UAV's task description. The flight phases in the task description were climb, ingress, loiter, egress, and descent. Yalcin [32] determined the performance parameters of an aircraft equipped with a turbofan engine for six different altitudes. Thermodynamic analysis was conducted by defining the relationship between fuel consumption and variable thrust.

Details of aircraft-engine pairing studies in the literature can be seen in Table 1. Table 1 shows that the engine is analyzed under three different conditions based on data obtained from articles. Analyses performed using experimental data are in a minority in the studies due to the difficulty of obtaining data. In addition, studies using experimental data include analyses performed at different operational modes at sea level. Most studies are performed by operating an engine at different operating modes on test rigs installed at sea level [13–16,29]. A number of studies have examined the following stages: LTO^{cycle}, or equivalent altitudes/operation modes [15,22]. Tona et al. [21] and Şöhret et al. [31], conducted the most detailed flight phase evaluation studies.

When Table 1 is examined, it can be seen that the analysis of the relationship between a commercial aircraft and engine, according to a defined real flight phase, has not been investigated in the open

literature. Therefore, this study has been conducted.

2. Design specifications details

2.1. Elaboration of aircraft-engine pairing

The B707 series was designed from the Boeing Model 367-80 prototype. The B707 series is divided into four different models. The B707-100/200 is designed for domestic flights and the B707-300/400 for international transport [33]. Views of the B707-300 for illustrative purposes only are shown in Fig. 1.

According to Roux [34], the air breathing engine model and type used in the B707 series is the JT3D series turbofan engine. Fig. 2 illustrates the three-dimensional model of the JT3D series turbofan engine with low bypass ratio applied as an air breathing propulsion component to the B707-320B/-320C, and the DC-8-62/-62F/-63/-63F. In addition, Fig. 2 comprises the views from the A-A sectional, the top, front and the perspective of the turbofan engine, respectively.

The diagrammatic illustration of the turbofan engine, designed using draw.io, is shown in Fig. 3. In Fig. 3, all of the components of the turbofan engine are shown together with station numbers. The JT3D series turbofan engine is comprised of a fan [1–2], an air compressor [AC/3–4], a combustion chamber [CC/4–6] and a gas turbine [GT/6–7]. A detailed station content of the turbofan engine, which is shown as a diagrammatic illustration in Fig. 3, is presented in Table 2. According to Table 2, air-combustion products (a-cp), which are flow line type core and streamline type primary, pass from AC(air)-CC(air + fuel)-GT(cp) components. The fan and the AC components of the turbofan engine comprise the cold section, the CC and the GT components form the hot section.

The characteristics of the JT3D turbofan engine are given in Table 3. The characteristics of JT3D series engines were obtained through research and referring to the literature [34,37–41]. The assumptions of the calculation and the input parameters requested by the software are obtained from Table 3. In addition, Table 3 contains the experimental data of the JT3D series engines.

2.2. Adopted flight phases

With the advance of technology, the development of software and applications has made aero-engines easy to model. In addition, the presence of easily-accessible, high measurement accuracy and reliable sensors facilitate data acquisition by different sectors (commercial, academic, educational) from aero-engines.

Classification of the flight phases and certain assumption parameters related to the analyses are shown in Table 4. The flight phases are divided into two parts. The first part is the 'so-called' LTO^{cycle} containing the taxi-out, take-off, climb-out, final approach, landing, and taxi-in flight phases. The second part is the 'so-called' CCD^{stage} containing the climb, cruise, and descent flight phases. The periods during which the flight phases occur are included in the analysis, taking into account both the ICAO and a busy airport in Europe. Table 4 also contains the flight phase points used in the analysis.

3. Method employed

3.1. Data acquisition

The data of the B707-JT3D pairing was initially collected from the literature and combined for use in the analysis (Tables 2–4). Data was obtained from the BADA (base of aircraft data), the ICAO, Bose [41] and Roux [34]. The data collected from the literature was converted to B707-JT3D performance parameters by GasTurb 12

Table 1

Details of aircraft-engine pairing studies in the literature.

Reference	Year	Airbreathing Engine Classification	Airbreathing Engine Type	Sector	Application	Altitudes ^{or} Flight Phases ^{or} Operation Modes
[10]	2006	Scramjet	N/A	N/A	N/A	Cruise
[11]	2007	Turbofan	F100-PW-100	Military	F-15	At sea level
[14]	2008	Turbojet	J69-T 25 A	Military	F-16 T-37B/C	11000 m *AoTC
[19]	2008	Turbofan	N/A	Commercial	N/A	N/A Takeoff Climbing Cruise Descent Holding Landing
[20]	2008	Turbofan	N/A	N/A	N/A	N/A
[12]	2009a	Turbofan	N/A	Commercial	B747/767, A300/310/330	N/A
[13]	2009b	Turbofan	CF6-80	N/A	N/A	At sea level
[21]	2010	Turbofan	N/A	Commercial	N/A	Takeoff Climb Cruise Descent Landing Holding
[22]	2012	Reciprocating engine	N/A	N/A	N/A	LTO (Takeoff, Climb-out, Approach, Taxi)
[25]	2012	Turboprop	CT7-9C	Military	N/A	N/A
[28]	2012	Turbofan	N/A	N/A	N/A	4000 m 5000 m 6000 m 7000 m 8000 m 9000 m
[15]	2013	Turboprop	T56	Military	C-130 Hercules	*AoTC 75% 100% Military Takeoff
[30]	2013	Turbofan	CF6-50	N/A	N/A	N/A
[26]	2014	Turbofan	PW6000	Commercial	A-318	Takeoff
[23]	2015a	Reciprocating engine	N/A	N/A	N/A	Cruise
[24]	2015b	Reciprocating engine	N/A	N/A	N/A	Cruise
[27]	2015	Turbofan	N/A	Commercial	N/A	N/A
[29]	2015	Turbofan	JT9D	Commercial	B747	at the maximum thrust operation mode
[31]	2015	Turbofan	N/A	Military and Civil	UAV	Climb Ingress Loiter Egress Descent
[32]	2017	Turbofan	N/A	N/A	N/A	0 3000 ft 17000 ft 20000 ft 27500 ft 35000 ft
[16]	2017a	Turbojet	J85	Military	T-38 F-5 NF-5	*AoTC Idle Intermediate Military Afterburner
[17]	2017b	Turbofan	PW4056	Commercial	B747	*AoTC Maximum Takeoff power Takeoff Running Power
[18]	2019	Turbofan	JT3D-3B	Commercial	N/A	N/A

^a AoTC: at the altitude where the test cell is located.

software via determining design parameters. The LTO^{cycle} and CCD^{stage} properties and assumptions of the B707-JT3D pairing are shown in Table 5. Table 5 is based on all flight phases performed by the B707-JT3D pairing.

Fig. 4, is used to determine the environmental conditions of the flight phases in Table 5. The ambient pressure and temperature, the

relative air density and the speed of sound according to varying altitudes are shown in Fig. 4.

Schematic representation of the flight phases used in the analysis is shown in Fig. 6. The ICAO defined aircraft movements below 3000 ft altitude as Landing and Take-off cycle (LTO^{cycle}) [42].

The mass flow rates of the B707-JT3D pairing in flight phases

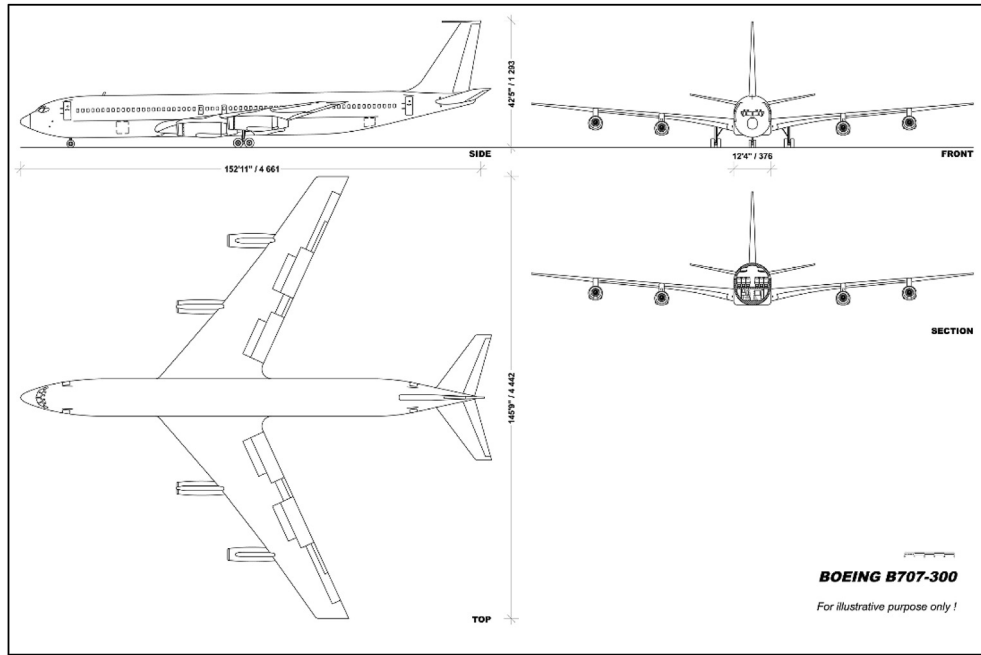


Fig. 1. Boeing 707-series typification by Boeing [33].

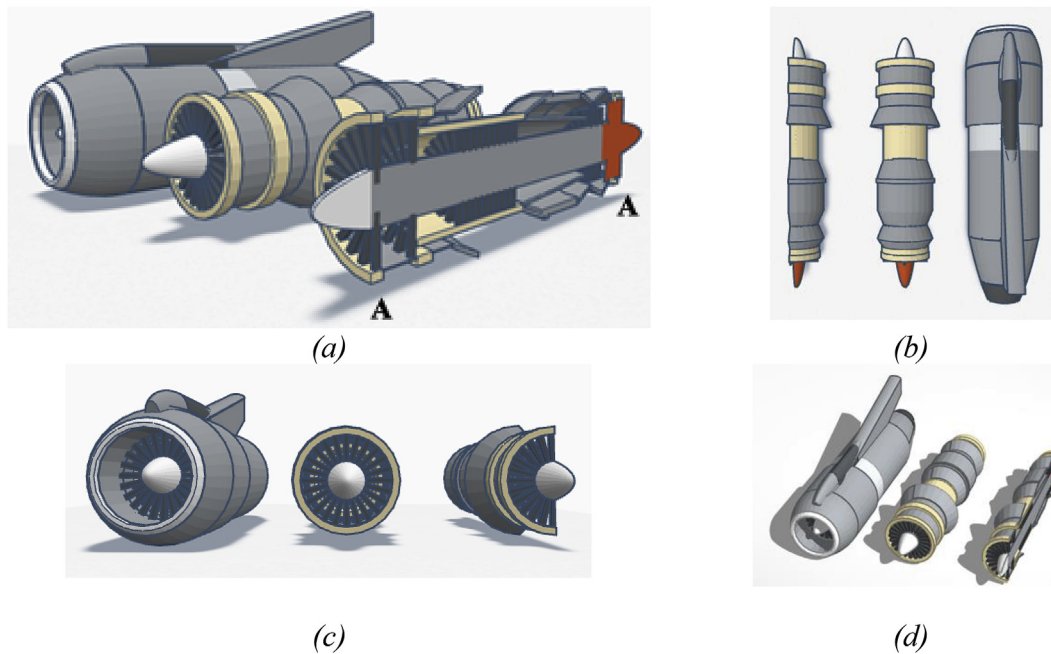


Fig. 2. A 3D model of an air breathing propulsion component; (a) A-A sectional view, (b) the view from the top, (c) the view from the front, (d) the view from the perspective [35].

and mass flow rates distribution according to flight phases are shown in Fig. 5. MFT , SN , a and f are symbolized mass flow type, station number, air and fuel respectively in Fig. 5.

3.2. Assumptions

The assumptions used when establishing the model are as follows.

- The data required to create the model was obtained from BADA, the ICAO, Bose [41] and Roux [34].
- The collected data was converted into cycle analyzes via Gas-Turb 12 software.
- The combustion process was considered to be complete combustion.
- Moisture was added to the combustion process.
- All components of B707-JT3D pairing were considered in the adiabatic process.
- It is assumed that the B707 uses JP-8 as fuel during flight. The chemical properties of JP-8 are assumed to be as follows; Chemical formula- $C_{11}H_{21}$, lower heating value-43370.596 (kJ/kg), H/C-1.91 [43–45].

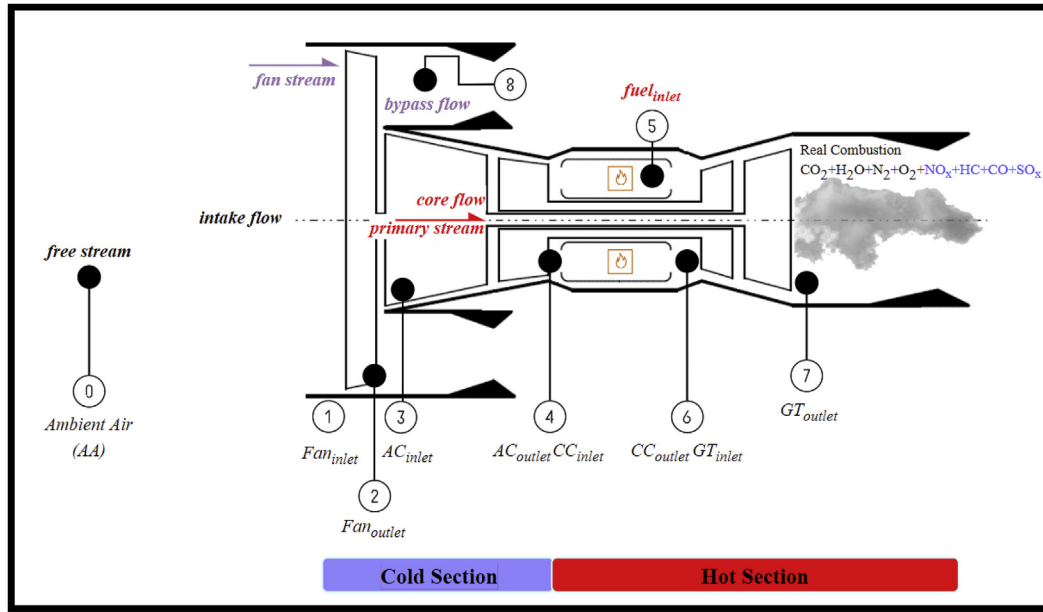


Fig. 3. The diagrammatic illustration of a turbofan engine [36].

Table 2
Station details of B707-JT3D pair.

Station Number	Location	Abbreviation	Flowline	Streamline	Mass Flow Type and Abbreviations	Section
0	Ambient Air	AA	Intake	Free	Air Flow \dot{m}_a	Cold
1	Fan-Inlet	Fan_{inlet}	Intake	Free	Air Flow \dot{m}_a	Cold
2	Fan-Outlet	Fan_{outlet}	Intake	Primary + Fan	Air Flow \dot{m}_a	Cold
3	Air Compressor-Inlet	AC_{inlet}	Core	Primary	Core Air Flow $\dot{m}_{a_{core}}$	Cold
4	Air Compressor-Outlet	AC_{outlet}	Core	Primary	Core Air Flow $\dot{m}_{a_{core}}$	Cold
share point	Combustion Chamber-inlet	CC_{inlet}				
5	Fuel-inlet	$fuel_{inlet}$	Core	—	Fuel Flow \dot{m}_f	Hot
6	Combustion Chamber-outlet	CC_{outlet}	Core	Primary	Combustion Product Flow \dot{m}_{cp}	Hot
share point	Gas Turbine-inlet	GT_{inlet}				
7	Gas Turbine-outlet	GT_{outlet}	Core	Primary	Combustion Product Flow \dot{m}_{cp}	Hot
8	Bypass flow	—	Bypass	Fan	Fan Flow $\dot{m}_{a_{fan}}$	Cold

- Dead state conditions were changed according to flight phase.
- Variable specific heats approach (*Exact Analysis*) was used to calculate specific heat capacities.
- Specific heat capacities were recalculated according to the changing conditions in each flight phase.
- The flight mission was described as a takeoff from an airport at sea level and landing at an airport at sea level.
- The flight times of climb, cruise and descent described as CCD^{stage} were assumed to be 10 min, 15 min, and 10 min, respectively.
- Pressure loss in the combustion chamber of the JT3D was modelled as 6% [46–48].

$$C_a H_\beta O_\gamma + \left(\alpha + \frac{\beta}{4} - \frac{\gamma}{2} \right) \times (O_2 + 3.76 N_2) + x H_2 O \rightarrow \alpha CO_2 + \left(\frac{\beta}{2} + x \right) H_2 O + 3.76 \left(\alpha + \frac{\beta}{4} - \frac{\gamma}{2} \right) N_2 \quad (1)$$

The specific heat capacity solutions of gases generated by combustion and contained in the air to essential for thermodynamic modeling of each defined flight phase are calculated according to the following equations [49–52].

$$\frac{\tilde{c}_{p,i}}{R_u} = \alpha_{i1} + \alpha_{i2} T + \alpha_{i3} T^2 + \alpha_{i4} T^3 + \alpha_{i5} T^4 \quad (2)$$

$$\frac{\tilde{h}_i}{R_u T} = \alpha_{i1} + \frac{\alpha_{i2}}{2} T + \frac{\alpha_{i3}}{3} T^2 + \frac{\alpha_{i4}}{4} T^3 + \frac{\alpha_{i5}}{5} T^4 + \frac{\alpha_{i6}}{T} \quad (3)$$

3.3. Mathematical modeling

Combustion equation employed to determine the air-fuel ratio of the flight path can be expressed as;

Table 3

Characteristics of JT3D series engines used in analysis [34,37–41].

Engine model	JT3D-1	JT3D-2	JT3D-3	JT3D-3A	JT3D-3B	JT3D-3C	JT3D-7
Aircraft	B707-120B/-120BF, B720B/BF, DC-8-51/-52	N/A	B707-120B/-320B/-320C, B720B, DC-8-51/-51F/-52/-52F/-53/-53F/-54/-54F/-55/-55F/-61/-61F/-62/-62F	N/A	B707-120B, B707-320B/BH/C/CH, B720B/BF, DC-8-53F/-55/-62/-62F, EC/RC-135, EC-24A	DC-8-50/61/61F/62/63, B707-120B/320B/C, B720B, VC-137C	B707-320B/-320C, DC-8-62/-62F/-63/-63F
Fan Diameter D_{fan} (m)	1.349	1.35	1.385	1.35	1.349	1.349	1.349
Engine Diameter D (m)	1.346	N/A	1.346	N/A	1.346	1.346	1.346
Engine mass m_{eng} (kg)	1880	1770	2170	1891	1950	1969	1969
Static sea level thrust without afterburner T_{ssl} (N)	75619	75700	80148	80200	80068	80068	84516
Specific fuel consumption at static sea level SFC_{ssl} [(kg/s)/kN]	0.0147	0.0147	0.0218	0.0151	0.0152	0.0145	0.0147
Air flow at static sea level $\dot{m}_{a,ssl}$ (kg/s)	204.1	196	236	196	207.7	204.1	214.1
Bypass ratio at static sea level	1.4	N/A	1.25	N/A	1.37	1.4	1.43
$BPR = \frac{\dot{m}_{fan}}{\dot{m}_{core}}$							
Fan pressure ratio FPR	N/A	N/A	1.75	N/A	1.74	1.66	1.82
Overall pressure ratio at static sea level OPR	12.5	13	16	13	13.6	13	13.5
Turbine inlet Temperature at static sea level TIT (K)	1150	N/A	1233	N/A	1144	N/A	N/A
Cruise thrust T_{cr} (N)	N/A	N/A	22300	N/A	N/A	N/A	N/A
Specific fuel consumption at cruise SFC_{cr} [(kg/s)/kN]	N/A	N/A	0.0216	N/A	N/A	N/A	N/A
Mach M_{cr}	0.85	N/A	0.8	N/A	N/A	N/A	N/A
Cruise altitude h_{cr} (m)	12192	N/A	10600	N/A	N/A	N/A	N/A

Table 4

Classification of flight phases and some assumption parameters related to the analyses.

	Flight Phase	Point	Description	Time-In Mode (ICAO) (hh:mm:ss)	Weighting (%)	A Busy European Airport (hh:mm:ss)	Weighting (%)	Thrust Setting at Sea Level (%)	
LTO ^{cycle}	Departure	Taxi-Out	1	<ul style="list-style-type: none">The first step is when the aircraft starts to leave the parked position under its own power.The second step is the taxiing to the runway. This terminates when the aircraft reaches the runway under its own power.The third step is preparation for take-off position. This starts from the entrance to the runway and ends when the aircraft reaches the take-off position.	00:26:00	79	00:20:06	74.44	7
		Take-Off	2	<ul style="list-style-type: none">The take-off phase includes all movement to an altitude of 35 feet from runway elevation.	00:00:42	2.07	00:00:42	2.59	100
		Climb-Out	3	<ul style="list-style-type: none">The climb phase is divided into two parts. (i) climb-out and (ii) climb. Climb-out is the flight phase between 3000 feet altitude and take-off phase.	00:02:12	6.68	00:02:12	8.15	85
	Arrival	Final Approach	7	<ul style="list-style-type: none">This phase is the last stage of the descent which is below 3000 feet.	00:04:00	12.15	00:04:00	14.81	30
		Landing	8	<ul style="list-style-type: none">The landing phase includes the movements from the final approach phase until leaving from the runway.					
CCD ^{stage}		Taxi-In	9	<ul style="list-style-type: none">Taxi-In begins leaving the runway and terminates upon arrival at the gate, apron or parking area.	total	total	total	total	7
		Climb	4	<ul style="list-style-type: none">The climb phase is divided into two parts. (i) climb-out and (ii) climb. Climb is the flight phase between a predetermined cruising altitude and 3000 feet altitude.	^a state variable	^a state variable	^a state variable	^a state variable	^a state variable
		Cruise	5	<ul style="list-style-type: none">The cruise phase, which is usually the longest section of a journey take places between the climb and descent phases.	^a state variable	^a state variable	^a state variable	^a state variable	^a state variable
		Descent	6	<ul style="list-style-type: none">The descent phase is like a reflection of the climb phase. The phase commences with altitude reduction from the cruise phase and it terminates when altitude reaches the 3000 feet LTO cycle zone.	^a state variable	^a state variable	^a state variable	^a state variable	^a state variable

^a CCD^{stage} time assumptions: Climb 00:10:00, Cruise 00:15:00, Descent 00:10:00.**Table 5**Properties and assumptions of LTO^{cycle} and CCD^{stage} of B707-JT3D pair.

Flight Phase	LTO ^{cycle}						CCD ^{stage}		
	Departure			Arrival			Climb	Cruise	Descent
Thrust (N)	5916	84516	71839	25355	25355	5916	71839	23516	25355
Altitude (m)	0	0 → 150	150 → 914.4	914.4 → 150	150 → 0	0	914.4 → 11 887.2	11 887.2	11 887.2 → 914.4
Temperature (K)	288.15	288.15 → 287	287 → 282.25	282.25 → 287	287 → 288.15	288.15	282.25 → 216.65	216.65	216.65 → 282.25
Pressure (kPa)	101.35	101.35 → 98.40	98.40 → 90.80	90.80 → 98.40	98.40 → 101.35	101.35	90.80 → 17.79	17.79	17.79 → 90.80
Density ($\sigma = \rho/\rho_0$)	1	1 → 0.97	0.97 → 0.91	0.91 → 0.97	0.97 → 1	1	0.91 → 0.26	0.26	0.26 → 0.91
Speed of Sound (km/h)	1224.17	1224.17 → 1218	1218 → 1211.2	1211.2 → 1218	1218 → 1224.17	1224.17	1211.2 → 1061.2	1061.2	1061.2 → 1211.2
Indicated Airspeed IAS (km/h)	N/A	241	296	463	260	N/A	538	870	556
Mach	N/A	0.2	0.24	0.38	0.21	N/A	0.76	0.82	0.75
Rate of Climb (km/h)	N/A	N/A	36.58	N/A	N/A	N/A	27.43	N/A	N/A
Rate of Descent (km/h)	N/A	N/A	N/A	27.43	N/A	N/A	N/A	N/A	54.86
\dot{m}_{fuel} (kg/s)	0.128	1.254	1.032	0.389	0.389	0.128	0.582	0.557	0.403
TSFC [(kg/s)/kN]	0.0216	0.0148	0.0144	$1.53 \cdot 10^{-5}$	$1.53 \cdot 10^{-5}$	0.0216	0.0081	0.0237	0.0159

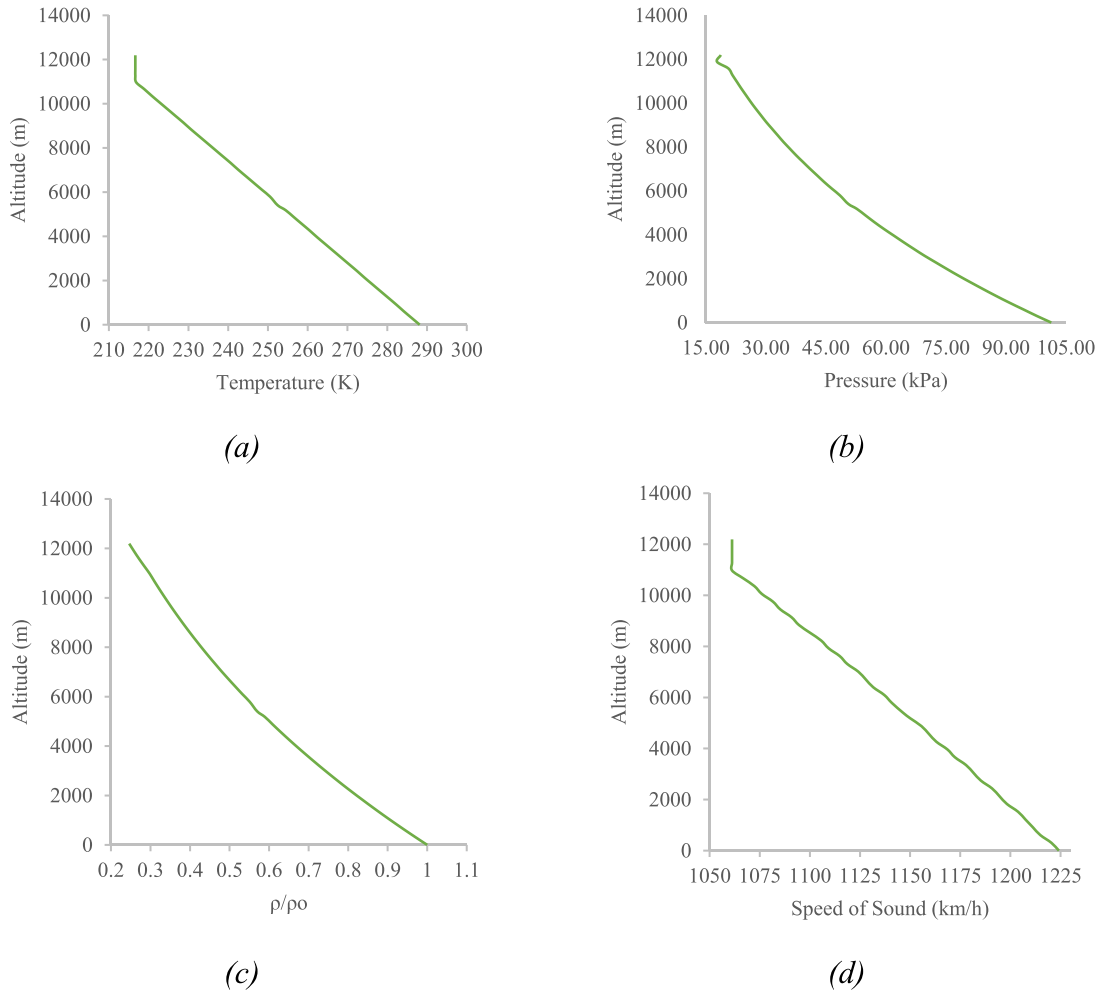


Fig. 4. Conditions of flight phases according to varying altitudes; (a) Altitude (m) – Temperature (K), (b) Altitude (m) – Pressure (kPa), (c) Altitude (m) – $\sigma = p/p_o$, (d) Altitude (m) – Speed of Sound (km/h).

$$\frac{\tilde{s}_i}{R_u} = \alpha_{i1} \ln T + \alpha_{i2} T + \frac{\alpha_{i3}}{2} T^2 + \frac{\alpha_{i4}}{3} T^3 + \frac{\alpha_{i5}}{4} T^4 + \alpha_{i7} \quad (4)$$

Matrices prepared from Shomate equations to calculate the specific heat capacity of each gas in air and combustion products were used depending on the changing ambient conditions under flight phases.

$$c_p(T) = \frac{N_{CO_2} M_{CO_2} c_{p,CO_2} + N_{CO} M_{CO} c_{p,CO} + N_{CH_4} M_{CH_4} c_{p,CH_4} + N_{H_2} M_{H_2} c_{p,H_2} + N_{NO} M_{NO} c_{p,NO} + N_{H_2O} M_{H_2O} c_{p,H_2O} + N_{NO_2} M_{NO_2} c_{p,NO_2} + N_{N_2} M_{N_2} c_{p,N_2} + N_{O_2} M_{O_2} c_{p,O_2}}{N_{CO_2} M_{CO_2} + N_{CO} M_{CO} + N_{CH_4} M_{CH_4} + N_{H_2} M_{H_2} + N_{NO} M_{NO} + N_{H_2O} M_{H_2O} + N_{NO_2} M_{NO_2} + N_{N_2} M_{N_2} + N_{O_2} M_{O_2}} \quad (5)$$

Coefficients of gas molecules in the air/combustion products at varying temperatures with the altitude changes under flight phases are shown in Table 6. The coefficients are different for each gas molecule at temperatures ranging from 300K to 5000K. Therefore, the enthalpy, entropy and specific heat capacity calculations of air and combustion products were obtained using the coefficients in Table 6. The solution reached using the coefficients in Table 6 is

described as the Exact Analysis. Equations concerning two different solutions of thermodynamic analysis of the JT3D are given in Table 7. Methods discussed in Table 7 are called analysis based on in-out and analysis based on fuel-product [11–13]. Where \dot{W} , \dot{E}_x are power and exergy, respectively.

4. Results and discussions

In this study, off-design parameters of a B707-JT3D pairing are collected from the literature and parametric cycles are created for each flight phase by means of GasTurb 12 software. In other words, data required to calculate flight path-efficiencies of the B707-JT3D in each flight phase is obtained using GasTurb 12 software.

Turbofan engine data, obtained through software and used in the thermodynamic analysis, is given in Table 8. In addition, the

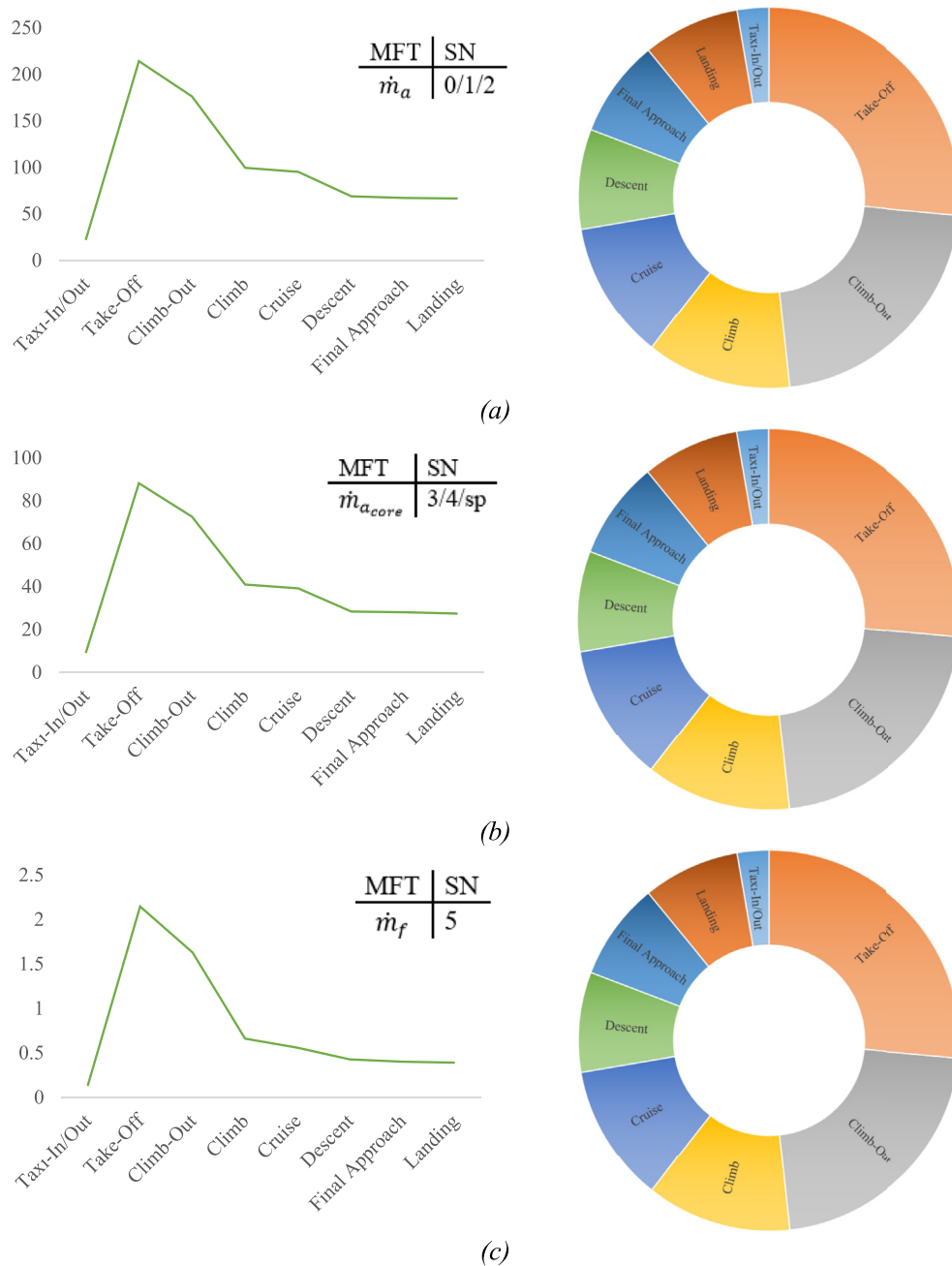


Fig. 5. Mass flow rates and mass flow distributions based on component station number under each flight phase; (a) air mass flow rates and distribution for station numbers 0/1/2, (b) core mass flow rates and distribution for station number 3/4/sp, (c) fuel mass flow rates and distribution for station number 5.

component station numbers and abbreviations of the JT3D are presented in Table 8.

The findings of the B707-JT3D pairing's analysis, based on the defined flight profile, are summarized as follows:

D represents the beginning of the sentence which includes explanations of this study's results and/or discussions based on other studies in the literature.

- Pressure and temperature values of the B707-JT3D pairing in all defined flight phases are presented in Table 8. The temperatures

and pressures in Table 8 are obtained from the graphs presented in section 3.1. Changes in both temperature and pressure values are presented depending on altitude.

- Furthermore, the results of the exergy rates (ph , ch , $total$) at nine flight phases are presented in Table 8. Table 8 is summarized as diacritical marks (a , b , c , d , e , f , g , h , i). Each of the diacritical marks corresponds to each of the flight phases. ^DSome of the data has been formed from data acquired by instrumentation of the engine-test rigs shared in the open literature and the remaining has been calculated by designed cycles through

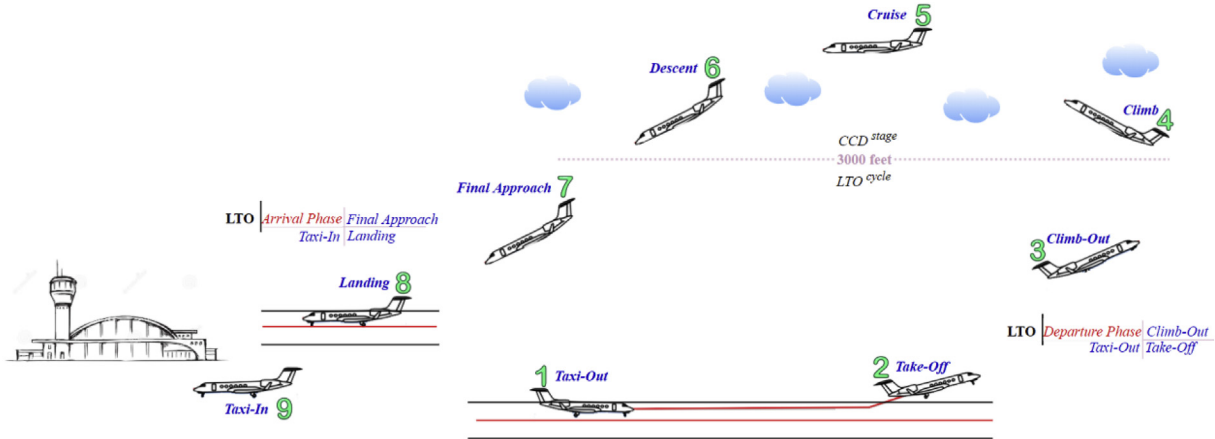


Fig. 6. Schematic representation of the flight phases used in the analysis.

Table 6

Coefficients of gas molecules in the air/combustion products at varying temperatures with the altitude changes under flight phases (revised from [50]).

Species	T range, K	α_{11}	α_{12}	α_{13}	α_{14}	α_{15}	α_{16}	α_{17}
CO ₂	1000–5000	0.44608(+1)	0.30982(-2)	-0.12393(-5)	0.22741(-9)	-0.15526(-13)	-0.48961(+5)	-0.98636
	300–1000	0.24008(+1)	0.87351(-2)	-0.66071(-5)	0.20022(-8)	0.63274(-15)	-0.48378(+5)	0.96951(+1)
H ₂ O	1000–5000	0.27168(+1)	0.29451(-2)	-0.80224(-6)	0.10227(-9)	-0.48472(-14)	-0.29906(+5)	0.66306(+1)
	300–1000	0.40701(+1)	-0.11084(-2)	0.41521(-5)	-0.29637(-8)	0.80702(-12)	-0.30280(+5)	-0.32270
CO	1000–5000	0.29841(+1)	0.14891(-2)	-0.57900(-6)	0.10365(-9)	-0.69354(-14)	-0.14245(+5)	0.63479(+1)
	300–1000	0.37101(+1)	-0.16191(-2)	0.36924(-5)	-0.20320(-8)	0.23953(-12)	-0.14356(+5)	0.29555(+1)
H ₂	1000–5000	0.31002(+1)	0.51119(-3)	0.52644(-7)	-0.34910(-10)	0.36945(-14)	-0.87738(+3)	-0.19629(+1)
	300–1000	0.30574(+1)	0.26765(-2)	-0.58099(-5)	0.55210(-8)	-0.18123(-11)	-0.98890(+3)	-0.22997(+1)
O ₂	1000–5000	0.36220(+1)	0.73618(-3)	-0.19652(-6)	0.36202(-10)	-0.28946(-14)	-0.12020(+4)	0.36151(+1)
	300–1000	0.36256(+1)	-0.18782(-2)	0.70555(-5)	-0.67635(-8)	0.21556(-11)	-0.10475(+4)	0.43053(+1)
N ₂	1000–5000	0.28963(+1)	0.15155(-2)	-0.57235(-6)	0.99807(-10)	-0.65224(-14)	-0.90586(+3)	0.61615(+1)
	300–1000	0.36748(+1)	-0.12082(-2)	0.23240(-5)	-0.63218(-9)	-0.22577(-12)	-0.10612(+4)	0.23580(+1)
OH	1000–5000	0.29106(+1)	0.95932(-3)	-0.19442(-6)	0.13757(-10)	0.14225(-15)	0.39354(+4)	0.54423(+1)
NO	1000–5000	0.31890(+1)	0.13382(-2)	-0.52899(-6)	0.95919(-10)	-0.64848(-14)	0.98283(+4)	0.67458(+1)
O	1000–5000	0.25421(+1)	-0.27551(-4)	-0.31028(-8)	0.45511(-11)	-0.43681(-15)	0.29231(+5)	0.49203(+1)
H	1000–5000	0.25(+1)	0.0	0.0	0.0	0.0	0.25472(+5)	-0.46012

software. The purpose of Table 8 is to determine the amount of exergy production and destruction within the components of the engine during the defined flight phases of the B707 commercial aircraft equipped with a JT3D turbofan engine.

- When the total exergy amounts are taken into consideration it can be seen that the exergy total has the highest value during the take-off flight phase. The throttle, whose task is to control the amount of fuel-air allowed to enter the engine, is located at the maximum position under take-off mode. The maximum throttle position causes as much fuel to be consumed as possible. For this reason, the take-off phase is to be the flight mode which consumes the most fuel of all the flight phases.

Therefore, the total amount of exergy with the highest value occurs during the take-off flight phase.

- Considering studies carried out to analyze aero-engine operations at different thrust power or various flight phases in the literature, the total amount of exergy is at a maximum in the operating mode that produces the highest thrust or during the flight phase requiring the highest thrust [15,16,19,21,22,31].
- The lowest value of the total exergy is the taxi-in/out flight phase in which the engine is operating under idle mode. The least fuel is consumed under the engine idle mode. Therefore, the total exergy is obtained under the engine idle mode.

Table 7

Method of evaluating the performance of the flight profile generated based on the off-design points: Thermodynamic analysis equations.





 Fan				 Air Compressor				 Combustion Chamber				 Gas Turbine			
In	Out	Fuel	Product	In	Out	Fuel	Product	In	Out	Fuel	Product	In	Out	Fuel	Product
$\dot{E}x_1 + \dot{W}_{fan}$	$\dot{E}x_2$	\dot{W}_{fan}	$\dot{E}x_2 - \dot{E}x_1$	$\dot{E}x_3 + \dot{W}_{AC}$	$\dot{E}x_4$	\dot{W}_{AC}	$\dot{E}x_4 - \dot{E}x_3$	$\dot{E}x_4 + \dot{E}x_5$	$\dot{E}x_6$	$\dot{E}x_5$	$\dot{E}x_6 - \dot{E}x_4$	$\dot{E}x_6$	$\dot{W}_{GT} + \dot{E}x_7$	$\dot{E}x_6 - \dot{E}x_7$	\dot{W}_{GT}

Table 8
Flight-path performance parameters of the B707-JT3D pairing during the flight scenario; (a) Taxi-Out, (b) Take-Off, (c) Climb-Out, (d) Climb, (e) Cruise, (f) Descent, (g) Final Approach, (h) Landing, (i) Taxi-In.

(a) Taxi-Out (i) Taxi-In								
Station Number	Abbreviation	Temperature (K)	Pressure (kPa)	ex_{ph} (kJ/kg)	ex_{ch} (kJ/kg)	$\dot{E}x_{ph}$ (kW)	$\dot{E}x_{ch}$ (kW)	$\dot{E}x_{total}$ (kW)
0	AA	288.15	101.35	—	—	—	—	—
1	Fan _{inlet}	288.15	101.35	—	—	—	—	—
2	Fan _{outlet}	364	184.45	58.11	—	1269.93	—	1269.931
3	AC _{inlet}	364	184.45	58.11	—	522.605	—	522.6052
4 share point	AC _{outlet}	938	2490.07	614.24	—	5524.09	—	5524.092
	CC _{inlet}	938	2490.07	614.24	—	5524.09	—	5524.092
5	fuel _{inlet}	288.15	101.35	—	46024.44	—	5891.13	5891.128
6 share point	CC _{outlet}	1086	2340.66	776.38	15.96	7081.66	145.532	7227.188
	GT _{inlet}	1086	2340.66	776.37	15.96	7081.56	145.532	7227.096
7	GT _{outlet}	809	173.38	303.28	15.96	2766.33	145.532	2911.864
(b) Take-Off								
0	AA	287	98.40	—	—	—	—	—
1	Fan _{inlet}	287	98.40	—	—	—	—	—
2	Fan _{outlet}	360	179	57.3	—	12267.9	—	12267.93
3	AC _{inlet}	360	179	57.3	—	5048.53	—	5048.53
4 share point	AC _{outlet}	942	2416.5	618.06	—	54455.4	—	54455.4
	CC _{inlet}	942	2416.5	618.06	—	54455.4	—	54455.4
5	fuel _{inlet}	288.15	101.35	—	46024.44	—	98722.4	98722.42
6 share point	CC _{outlet}	1415	2271.51	1119.98	15.69	101080	1416.05	102496.5
	GT _{inlet}	1415	2271.51	1119.98	15.69	101080	1416.05	102496.5
7	GT _{outlet}	1102	168.26	575.02	15.69	51896.7	1416.05	53312.76
(c) Climb-Out								
0	AA	282.25	90.8	—	—	—	—	—
1	Fan _{inlet}	282.25	90.8	—	—	—	—	—
2	Fan _{outlet}	352	165.26	55.98	—	9863.52	—	9863.515
3	AC _{inlet}	352	165.26	55.98	—	4059.06	—	4059.06
4 share point	AC _{outlet}	871	2230.95	560.88	—	40668.9	—	40668.91
	CC _{inlet}	871	2230.95	560.88	—	40668.9	—	40668.91
5	fuel _{inlet}	288.15	101.35	—	46024.44	—	74973.8	74973.81
6 share point	CC _{outlet}	1394	2097.09	1101.83	16.76	81687.6	1242.55	82930.14
	GT _{inlet}	1394	2097.09	1101.83	16.76	81687.6	1242.55	82930.14
7	GT _{outlet}	1090	155.34	568.76	16.76	42166.8	1242.55	43409.34
(d) Climb								
0	AA	216.65	17.79	—	—	—	—	—
1	Fan _{inlet}	216.65	17.79	—	—	—	—	—
2	Fan _{outlet}	269	32.38	47.72	—	4741.79	—	4741.793
3	AC _{inlet}	269	32.38	47.72	—	1951.35	—	1951.355
4 share point	AC _{outlet}	682	437.13	430.97	—	17623.1	—	17623.12
	CC _{inlet}	682	437.13	430.97	—	17623.1	—	17623.12
5	fuel _{inlet}	288.15	101.35	—	46024.44	—	30330.1	30330.11
6 share point	CC _{outlet}	1060	410.9	813.73	31.52	33811.1	1309.68	35120.78
	GT _{inlet}	1060	410.9	813.73	31.52	33811.1	1309.68	35120.78
7	GT _{outlet}	818	30.44	397.9	31.52	16533	1309.68	17842.73
(e) Cruise								
0	AA	216.65	17.79	—	—	—	—	—
1	Fan _{inlet}	216.65	17.79	—	—	—	—	—
2	Fan _{outlet}	268	32.38	42.52	—	4043.59	—	4043.594
3	AC _{inlet}	268	32.38	42.52	—	1664.03	—	1664.031
4 share point	AC _{outlet}	667	437.13	419.34	—	16411	—	16410.97
	CC _{inlet}	667	437.13	419.34	—	16411	—	16410.97
5	fuel _{inlet}	288.15	101.35	—	46024.44	—	25635.6	25635.61
6 share point	CC _{outlet}	996	410.9	743.81	31.52	29523.5	1251.1	30774.59
	GT _{inlet}	996	410.9	743.81	31.52	29523.5	1251.1	30774.59
7	GT _{outlet}	743	30.44	329.52	31.52	13079.4	1251.1	14330.49
(f) Descent								
0	AA	282.25	90.8	—	—	—	—	—
1	Fan _{inlet}	282.25	90.8	—	—	—	—	—
2	Fan _{outlet}	347.1	165.26	55.03	—	3786.38	—	3786.376
3	AC _{inlet}	347.1	165.26	55.03	—	1558.18	—	1558.179
4 share point	AC _{outlet}	786	2230.95	494.4	—	13999	—	13998.98
	CC _{inlet}	786	2230.95	494.4	—	13999	—	13998.98
5	fuel _{inlet}	288.15	101.35	—	46024.44	—	19606.4	19606.41
6 share point	CC _{outlet}	1139	2097.09	834.35	16.76	23980.1	481.701	24461.83
	GT _{inlet}	1139	2097.09	834.35	16.76	23980.1	481.701	24461.83
7	GT _{outlet}	824	155.34	321.97	16.76	9253.77	481.701	9735.468

Table 8 (continued)

(g) Final Approach								
0	AA	287	98.4	—	—	—	—	—
1	Fan _{inlet}	287	98.4	—	—	—	—	—
2	Fan _{outlet}	361	179	64.99	—	4316.34	—	4316.336
3	AC _{inlet}	361	179	64.99	—	1776.27	—	1776.27
4 share point	AC _{outlet}	899	2416.5	404.96	—	11068.1	—	11068.14
	CC _{inlet}	899	2416.5	404.96	—	11068.1	—	11068.14
5	fuel _{inlet}	288.15	101.35	—	46024.44	—	17903.5	17903.51
6 share point	CC _{outlet}	1062	2271.51	628.82	15.69	17431.2	434.934	17866.1
	GT _{inlet}	1062	2271.51	628.82	15.69	17431.2	434.934	17866.1
7	GT _{outlet}	792	168.26	290.8	15.69	8061.1	434.934	8496.037
(h) Landing								
0	AA	288.15	101.35	—	—	—	—	—
1	Fan _{inlet}	288.15	101.35	—	—	—	—	—
2	Fan _{outlet}	364	184.45	58.11	—	1269.93	—	1269.931
3	AC _{inlet}	364	184.45	58.11	—	522.605	—	522.6052
4 share point	AC _{outlet}	938	2490.07	614.24	—	5524.09	—	5524.092
	CC _{inlet}	938	2490.07	614.24	—	5524.09	—	5524.092
5	fuel _{inlet}	288.15	101.35	—	46024.44	—	5891.13	5891.128
6 share point	CC _{outlet}	1086	2340.66	776.38	15.96	7081.66	145.532	7227.188
	GT _{inlet}	1086	2340.66	776.37	15.96	7081.56	145.532	7227.096
7	GT _{outlet}	809	173.38	303.28	15.96	2766.33	145.532	2911.864

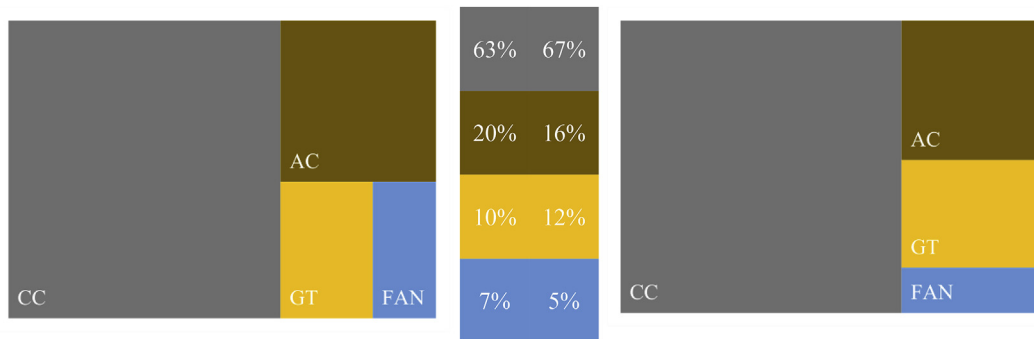


Fig. 7. Distribution and percentages of exergy destruction based on the components during taxi-in/out (left) and take-off (right).

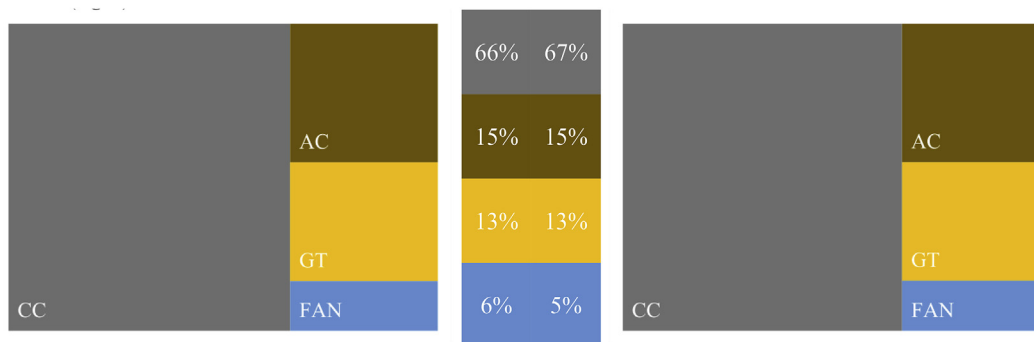


Fig. 8. Distribution and percentages of exergy destruction based on the components during climb-out (left) and climb (right).

Similarly, the lowest exergy total occurs when the engine is exposed to the lowest power setting.

- In Figs. 7–11, detailed maps of exergy destruction for each flight phase are presented. ^dIt does not matter whether the exergy destruction calculation is the In/Out or the Fuel/Product method. The behavior of the method used in the calculation of exergy destruction is identification of the parts entering and exiting. The definitions of the entering and exiting parts according to both methods are different. Although the definitions

are different, the same result is reached due to subtraction of the entry and exit in the exergy destruction calculation [11].

- The figurative representation represents the component-based exergy destruction rates. In addition to the figurative representation, the percentages of exergy destruction for each component under the flight phase are given (Figs. 7–10).
- As a result of the parametric cycle of the B707-JT3D, Taxi-In and Taxi-Out data was obtained as equivalent. ^dThe reason why Taxi-In and Taxi-Out data is obtained as equivalent is due to the fact

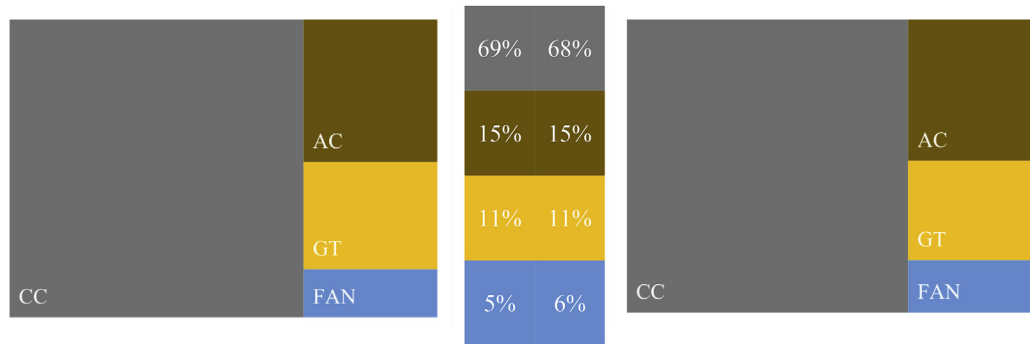


Fig. 9. Distribution and percentages of exergy destruction based on the components during cruise (left) and descent (right).

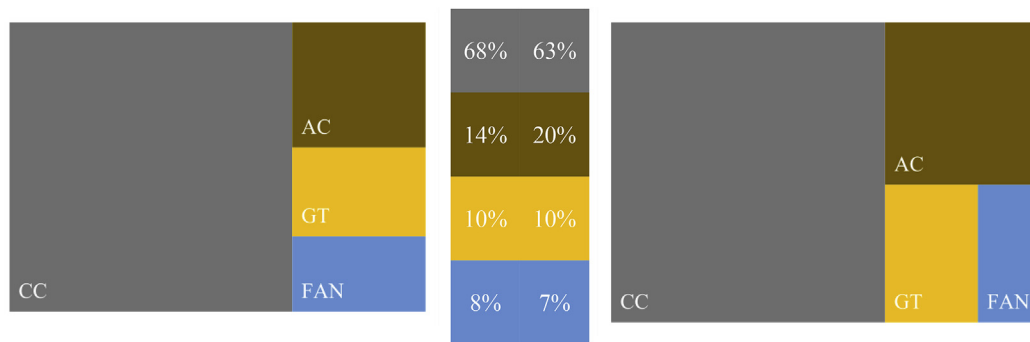


Fig. 10. Distribution and percentages of exergy destruction based on the components during final-approach (left) and landing (right).

that the aircraft uses approximately the same thrust power (*the setting of the aircraft throttle*) both when exiting and when approaching the apron (ICAO).

- In Fig. 7, the exergy destruction rates of Fan, AC, CC and GT have been calculated as 7%, 20%, 63% and 10% during Taxi-In/Out of Flight phases, respectively. In addition, the exergy destruction rates of Fan, AC, CC and GT have been calculated as 5%, 16%, 67% and 12%, respectively, under Take-Off flight mode (Fig. 7). In addition, the exergy destruction rates of Climb-Out, Climb, Cruise, Descent, Final Approach and Landing due to flight phase-component pairing are given in Figs. 8–10, respectively. In this study, the combustion chamber was found to be the component with the most exergy destruction among aircraft engine components as in other studies in which thermodynamic analysis of different aircraft engines was performed. The exposure of gases to high-temperature, friction and flutter occurring throughout the combustion reaction generate an irreversible process within the combustion chamber. An irreversible process is the production of entropy (*exergy destruction*). In addition, the highest and lowest values of exergy destruction rate have been calculated CC and Fan, respectively [11,15,25].
- In addition to the graph of the component's exergy destruction calculated with reference to flight phases presented in Figs. 7–10, graphs of the flight phases' exergy destruction based on components have been prepared to better evaluate the exergy destruction of each flight phase of the B707-JT3D pairing (Fig. 11). Moreover, function estimation was applied to exergy destruction rates occurring at each flight phase of the four components mentioned in Fig. 11 to take the lead over other studies and for easy comparison with other aircraft-engine pairing studies. Function estimation based on components was performed using various regression models. The regression models used in estimation are ab-exponential, cubic,

exponential, hyperbolic, linear, logarithmic, quadratic and power. Therefore, the best-defined function that can be used in future studies is determined and presented to the literature. Function estimation results resulting from the calculations made with the regression models mentioned above were compared in terms of correlation-determination coefficients and average relative error. Dependent and independent variables were defined to form the model of the exergy destruction amounts of the components in each flight phase. The dependent variable was determined as the amount of exergy destruction of each component in each flight phase, and the independent variable was selected as the throttle setting (thrust power) connected with altitude.

- The exergy destruction function having the lowest average relative error and highest correlation and determination coefficient was best estimated with a cubic regression model applied among all of the regression models for the nine flight phase data. The correlation coefficient, coefficient of determination, and the average relative error were calculated as 0.9908, 0.9818, 11.43%, respectively (Fig. 11a). The amount of exergy destruction for the Fan in the nine flight phases can be calculated from the following formula with 11.43% error and 0.99 sensitivity;

$$y = 0.0199x^3 - 2.6000x^2 + 102.3292x - 121.2263$$

- The correlation coefficient, coefficient of determination, and the average relative error were calculated as 0.9993, 0.9986, 3.09%, respectively (Fig. 11b). The amount of exergy destruction for the AC in the nine flight phases can be calculated from the following formula with 3.09% error and 0.99 sensitivity;

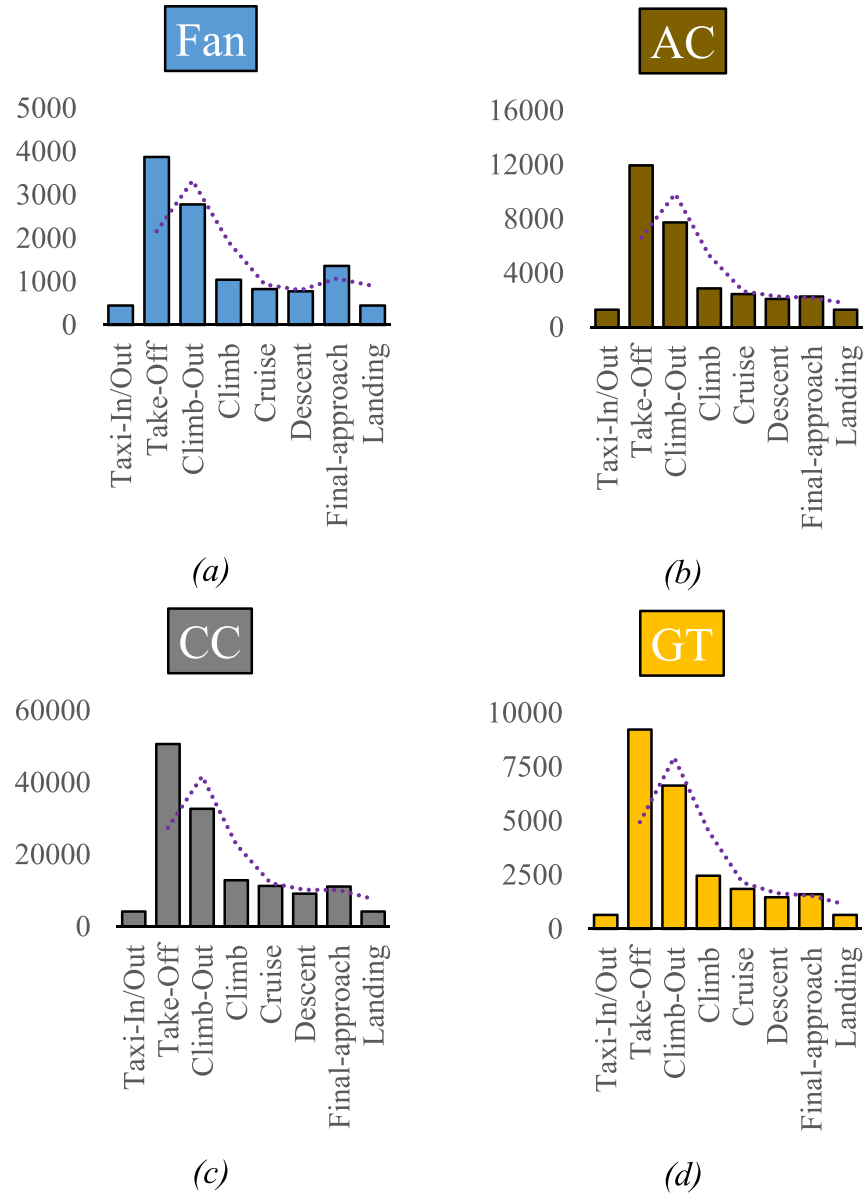


Fig. 11. Comparative presentation of exergy destruction rates at nine flight phases and determination of the function approximation by applying regression analysis to the obtained exergy destruction data: (a) Fan, (b) AC, (c) CC, (d) GT.

Table 9

The exergy efficiency of the JT3D components at various flight phases according to two different thermodynamic efficiency calculation methods.

Components	Exergy Efficiency							
	Fan		AC		CC		GT	
	In Out	Fuel Product	In Out	Fue Product	In Out	Fue Product	In Out	Fuel Product
Taxi-In/Out	0.74	0.75	0.81	0.8	0.63	0.29	0.91	0.86
Take-Off	0.76	0.76	0.82	0.8	0.68	0.49	0.91	0.82
Climb-Out	0.78	0.78	0.84	0.82	0.72	0.56	0.92	0.82
Climb	0.82	0.84	0.86	0.83	0.73	0.58	0.93	0.86
Cruise	0.83	0.83	0.87	0.85	0.73	0.56	0.94	0.88
Descent	0.83	0.83	0.87	0.86	0.73	0.54	0.94	0.9
Final Approach	0.76	0.77	0.83	0.78	0.63	0.38	0.91	0.88
Landing	0.74	0.75	0.81	0.8	0.63	0.29	0.91	0.86

$$y = 0.0408x^3 - 4.5695x^2 + 164.0378x + 354.1863$$

- The correlation coefficient, coefficient of determination, and the average relative error were calculated as 0.9989, 0.9978, 4.16%, respectively (Fig. 11c). The amount of exergy destruction for the CC in the nine flight phases can be calculated from the following formula with 4.16% error and 0.99 sensitivity;

$$y = 0.1984x^3 - 24.1076x^2 + 944.3706x - 1281.0239$$

- The correlation coefficient, coefficient of determination, and the average relative error were calculated as 0.9975, 0.9950, 8.86%, respectively (Fig. 11d). The amount of exergy destruction for the GT in the nine flight phases can be calculated from the following formula with 8.86% error and 0.99 sensitivity;

$$y = 0.0251x^3 - 2.5489x^2 + 96.6024x - 117.0344$$

- It is understood that if the amount of flight data required for exergy destruction calculations of the same components at different flight phases increases, function prediction with low average relative errors can be made for certain types of engines (turbojet, turbofan, turboprop, reciprocating). In the literature, if the number of articles related to aircraft-engine pairings increases, the functions of the entropy production behavior of the components of the engines at certain altitudes can be formed by the data obtained from the studies.
- The exergy efficiency of the JT3D components at various flight phases according to two different thermodynamic efficiency calculation methods are shown in Table 9. The most inefficient component at each flight phase was found to be the combustion chamber by both thermodynamic efficiency calculation methods [11,15,25].

5. Conclusion

The studies conducted considering the relationship between aircraft and engine pairings provide meaningful and useful information. In addition, thermodynamic analysis to be performed on the engine, by determining the flight conditions and the route of the aircraft in which the engine is equipped, will provide additional information in order to improve the process.

Concluding remarks obtained from the results of this study may be listed as follows:

- The necessity of making the data of aircraft-engine pairings easily accessible has emerged. Making aircraft-engine data, that the academic community uses to perform environmental impact, sustainability, optimization and similar analyses, more accessible will contribute to both aircraft/engine design companies and airline companies that use the aircraft-engine pairing commercially.
- Functional estimation may be performed in addition to thermodynamic analysis when sufficient experimental and short-range data is accessed. If the method is applied to many aircraft-engine pairings, thermodynamic performance parameters can be calculated directly by means of a single function for specific aircraft and engines.
- Performing performance analysis of aero-engines without fitting them to aircraft will mean obtaining results far from the

performance parameters of actual flight conditions. This study presents the necessity of determining the performance parameters of the engine in the aircraft-engine relationship.

The results of the study can contribute to academicians, designers and manufacturers. The study is expected to contribute to the academic field in terms of data and function estimation. As a result, the compatibility of the engine data obtained in future studies, or whether it belongs to a template, can be investigated by the function estimation method. Moreover, the methodology and results of this paper may be beneficial to engineers and researchers dealing with the analysis and suitability of aircraft-engine pairings.

References

- [1] Bağan H, Gereide E. Use of a nominal group technique in the exploration of safety hazards arising from the outsourcing of aircraft maintenance. *Saf Sci* 2019;118:795–804.
- [2] Odoni A. The international institutional and regulatory environment. *Global Airline Indust* 2009;19–46.
- [3] de Oliveira S. Exergy method for conception and assessment of aircraft systems. In: *Exergy*. London: Springer; 2013. p. 237–79.
- [4] Le Goff P. In: Brodyansky VM, Sorin MV, editors. The efficiency of industrial processes: exergy analysis and optimization. Amsterdam: Elsevier; 1994. p. 18–9.
- [5] Roth B, McDonald R, Mavris D. A method for thermodynamic work potential analysis of aircraft engines. In: 38th AIAA/ASME/SAE/ASEE joint propulsion conference & exhibit; 2002. p. 3768.
- [6] Moorhouse DJ. Proposed system-level multidisciplinary analysis technique based on exergy methods. *J Aircr* 2003;40(1):11–5.
- [7] Roth B. Work transfer analysis of turbojet and turbofan engines. In: 40th AIAA/ASME/SAE/ASEE joint propulsion conference and exhibit; 2004. p. 4077.
- [8] Roth B. A work transfer perspective of propulsion system performance. In: 40th AIAA/ASME/SAE/ASEE joint propulsion conference and exhibit; 2004. p. 4079.
- [9] Bejan A, Siems DL. The need for exergy analysis and thermodynamic optimization in aircraft development. *Exergy An Int J* 2001;1(1):14–24.
- [10] Amati V, Bruno C, Simone D, Sciubba E. Development of a novel modular simulation tool for the exergy analysis of a scramjet engine at cruise condition. *Int J Thermodyn* 2006;9(4):181–91.
- [11] Turgut ET, Karakoc TH, Hepbasli A. Exergetic analysis of an aircraft turbofan engine. *Int J Energy Res* 2007;31(14):1383–97.
- [12] Turgut ET, Karakoc TH, Hepbasli A. Exergoeconomic analysis of an aircraft turbofan engine. *Int J Exergy* 2009a;6(3):277–94.
- [13] Turgut ET, Hikmet Karakoc T, Hepbasli A, Rosen MA. Exergy analysis of a turbofan aircraft engine. *Int J Exergy* 2009b;6(2):181–99.
- [14] Balli O, Aras H, Aras N, Hepbasli A. Exergetic and exergoeconomic analysis of an aircraft jet engine (AJE). *Int J Exergy* 2008;5(5):567.
- [15] Balli O, Hepbasli A. Energetic and exergetic analyses of T56 turboprop engine. *Energy Convers Manag* 2013;73:106–20.
- [16] Balli O. Exergetic, exergoeconomic, sustainability and environmental damage cost analyses of J85 turbojet engine with afterburner. *Int J Turbo Jet Engines* 2017. <https://doi.org/10.1515/tjj-2017-0019>. Published Online: 2017-06-21.
- [17] Balli O. Exergy modeling for evaluating sustainability level of a high by-pass turbofan engine used on commercial aircrafts. *Appl Therm Eng* 2017b;123:138–55.
- [18] Balli O. Advanced exergy analysis of a turbofan engine (TFE): splitting exergy destruction into unavoidable/avoidable and endogenous/exogenous. *Int J Turbo Jet Engines* 2019;36(3):305–27.
- [19] Gandolfi R, Pellegrini L, Silva G, Oliveira S. January). Exergy analysis applied to a complete flight mission of commercial aircraft. In: 46th AIAA aerospace sciences meeting and exhibit; 2008. p. 153.
- [20] Struchtrup H, Elfring GJ. External losses in high-bypass turbo fan air engines. *Int J Exergy* 2008;5(4):400–12.
- [21] Tona C, Raviolo PA, Pellegrini LF, de Oliveira Júnior S. Exergy and thermoeconomic analysis of a turbofan engine during a typical commercial flight. *Energy* 2010;35(2):952–9.
- [22] Altuntas O, Karakoc TH, Hepbasli A. Exergetic, exergoeconomic and sustainability assessment of piston-prop aircraft engine. *J Therm Sci Technol* 2012;32(2):133–43.
- [23] Altuntas O, Karakoc TH, Hepbasli A. A parametric study of a piston-prop aircraft engine using exergy and exergoeconomic analysis methods. *Int J Green Energy* 2015a;12(1):2–14.
- [24] Altuntas O, Karakoc TH, Hepbasli A. Exergoeconomic environmental optimization of piston-prop aircraft engines. *Int J Green Energy* 2015b;12(1):41–50.
- [25] Aydin H, Turan O, Midilli A, Karakoc TH. Exergetic and exergoeconomic analysis of a turboprop engine: a case study for CT7–9C. *Int J Exergy* 2012;11(1):69–88.
- [26] Aydin H, Turan O, Karakoc TH, Midilli A. Sustainability assessment of PW6000 turbofan engine: an exergetic approach. *Int J Exergy* 2014;14(3):388–412.

- [27] Aydin H, Turan O, Karakoc TH, Midilli A. Exergetic sustainability indicators as a tool in commercial aircraft: a case study for a turbofan engine. *Int J Green Energy* 2015;12(1):28–40.
- [28] Turan O. Effect of reference altitudes for a turbofan engine with the aid of specific–exergy based method. *Int J Exergy* 2012;11(2):252–70.
- [29] Turan O. An exergy way to quantify sustainability metrics for a high bypass turbofan engine. *Energy* 2015;86:722–36.
- [30] Hassan HZ. Evaluation of the local exergy destruction in the intake and fan of a turbofan engine. *Energy* 2013;63:245–51.
- [31] Şöhret Y, Dinç A, Karakoç TH. Exergy analysis of a turbofan engine for an unmanned aerial vehicle during a surveillance mission. *Energy* 2015;93: 716–29.
- [32] Yalcin E. Thrust performance evaluation of a turbofan engine based on exergetic approach and thrust management in aircraft. *Int J Turbo Jet Engines* 2017;34(2):177–86.
- [33] Boeing. 707 airplane characteristics airport planning. The Boeing Company Commercial Airplane Division; 2010. D6-58322.
- [34] Roux E. Turbofan and turbojet engines: database handbook. 2007.
- [35] tinkercad.com. accessed 08.07.19, <https://www.tinkercad.com/>.
- [36] draw.io. accessed 12.07.19, <https://www.draw.io/>.
- [37] McRae GM. Refanned commercial gas turbine engines. *SAE Trans* 1973: 1123–9.
- [38] Gray DE. Study of turbofan engines designed for low energy consumption. NASA CR-135002 PWA-5318. 1976.
- [39] Neitzel RE, Hirschkron R, Johnston RP. Study of turbofan engines designed for low enery consumption. 1976. NASA CR135053R76AEG432.
- [40] Waters MH, Schairer ET. Analysis of Turbofan propulsion system weight and dimensions. 1977. p. 199. NASA TM X-73.
- [41] Bose T. Airbreathing propulsion. Springer; 2012.
- [42] Winther M, Rypdal K, Sørensen L, Kalivoda M, Bukovnik M, Kilde N, Box L. EMEP/EEA air pollutant emission inventory guidebook 2016–Update July 2017–1. 2017. A. 3. a, 1. A. 5. b Aviation.
- [43] Edwards T, ve Maurice LQ. Surrogate mixtures to represent complex aviation and rocket fuels. *J Propuls Power* 2001;17(No. 2):461–6.
- [44] Violi A, Yan S, Eddings EG, Sarofim AF, Granata S, Faravelli T, ve Ranzi E. Experimental formulation and kinetic model for JP-8 surrogate mixtures. *Combust Sci Technol* 2002;174:399–417.
- [45] Aerospace SAE. ARP1533B revision A, procedure for the analysis and evaluation of gaseous emissions from aircraft engines. Technical report; 2013. <https://www.sae.org/standards/content/arp1533b/>.
- [46] Roth BA, ve Mavis DN. A comparison of thermodynamic loss models applied to the J-79 turbojet engine. In: Joint propulsion conference and exhibit. 36th. Alabama, USA: Huntsville; 2000. AIAA2000-3715.
- [47] Lefebvre AH, Ballal DR. Gas turbine combustion: alternative fuels and emissions. 3rd ed. London: CRC Press; 2010.
- [48] Boyce MP. Gas turbine engineering handbook. 4nd ed. Elsevier; 2012.
- [49] Gordon S, ve McBride BJ. Computer program for the calculation of complex chemical equilibrium composition, rocket performance, incident and reflected shocks and Chapman Jouguet detonations. NASA Publication SP-273; 1971. NTIS number N71-37775.
- [50] Heywood JB. Internal combustion engine fundamentals. New York: McGraw-Hill; 1988.
- [51] McBride BJ, Gordon S, ve Reno MA. Coefficients for calculating thermodynamic and transport properties of individual species. NASA Tech Memo 1993;4513.
- [52] McBride BJ, Zehe MJ, ve Gordon S. NASA Glenn coefficients for calculating thermodynamic properties of individual species. 2002. NASA/TP–2002–211556.